Available online at www.sciencedirect.com
SCIENCE DIRECT
Planetary and Space Science 54 (2006) 456–471
Planetary and Space Science
www.elsevier.com/locate/pss

ICE, the electric field experiment on DEMETER

J.J. Berthelier[a,*], M. Godefroy[a], F. Leblanc[a], M. Malingre[a], M. Menvielle[a], D. Lagoutte[b], J.Y. Brochot[b], F. Colin[b], F. Elie[b], C. Legendre[b], P. Zamora[b], D. Benoist[c], Y. Chapuis[c], J. Artru[d], R. Pfaff[e]

[a]*CETP/IPSL, 4 Avenue de Neptune, 94107, SAINT-MAUR, France*
[b]*LPCE, 3A Avenue de la Recherche Scientifique, 45071 ORLEANS Cedex 2, France*
[c]*Observatoire de Nançay, 18330 Nançay, France*
[d]*JPL/CALTECH, PASADENA, USA*
[e]*GSFC/NASA, GREENBELT, MD, USA*

Received 2 March 2005; received in revised form 3 October 2005; accepted 14 October 2005

Abstract

The objective of the ICE (Instrument Champ Electrique) experiment on board DEMETER is to provide a nearly continuous survey of the electromagnetic and/or electrostatic waves that may arise from the coupling of seismic activity with the upper atmosphere and ionosphere. To this aim it makes use of 4 spherical electrodes with embedded preamplifiers that are deployed by stacer booms at approximately 4 m from the satellite. Measurements are made over a wide frequency range from DC to 3.175 MHz, subdivided in the signal processing unit in four frequency channels DC/ULF, ELF, VLF and HF. Three axis measurements are available in the DC/ULF range for all modes of operation of DEMETER and in the ELF range in the DEMETER Burst modes. In the VLF and HF ranges and in ELF during DEMETER Survey modes only one axis of measurement is available that can be selected by telecommand. We present in this paper a general description of the instrument and its modes of operation and in-flight performances. The sensitivity is ~0.1–0.2 μV/m $Hz^{1/2}$ from ~100 Hz through the HF range and the dynamical range is >80 dB in ELF and VLF and about 42 dB in HF. In order to illustrate the instrument capabilities, we briefly describe a number of observations from the first months of operation in various regions along the orbit from the equator to high latitudes.

Keywords: DC/AC electric field sensors; Ionospheric plasma waves; Ionospheric turbulence; Ionospheric effects of seismsic activity

1. Introduction

In the last 20 years a number of papers have reported the detection of natural electromagnetic signals related to Earth's seismic activity, mainly from ground-based receivers but also from satellite experiments. The corresponding observations cover a wide range of frequencies with measurements gathered at ULF (Fraser-Smith et al., 1990; Molchanov et al., 1992; Hayakawa et al., 2000), ELF and VLF (Molchanov et al., 1993; Parrot, 1995; Singh et al., 2000, see also reviews by Molchanov et al., 1993; Hayakawa, 1997), LF and HF (Biagi, 1999; Takano et al., 2002) and even recently in the VHF range (Yamada et al., 2002). In addition, a number of observations have been published indicating that, before or during the time of earthquakes, disturbances may affect the propagation characteristics of high power transmitters in the VLF range (Hayakawa et al., 1996; Molchanov et al., 1998; Ohta et al., 2000; Nagao et al., 2002) and, possibly, in the VHF range (Sakai et al., 2001). In many cases, not only the understanding of the phenomena but also their proper characterization has proven to be difficult due to the weakness of the signals, the relative paucity of observations and hence their subsequent lack of meaningful statistics, and the difficulty of removing other natural signals that can mix with, and indeed sometimes mask, those induced by seismic activity. As described in Parrot et al. (2005), the goal of the DEMETER mission is to provide a nearly continuous survey of natural electrostatic and

*Corresponding author. Tel.: +33 1 4511 4242; fax: +33 1 4889 4433.
E-mail address: Jean-Jacques.berthelier@cetp.ipsl.fr (J.J. Berthelier).

0032-0633/$ - see front matter © 2006 Elsevier Ltd. All rights reserved.
doi:10.1016/j.pss.2005.10.016

electromagnetic emissions as well as ionospheric irregularities that can be related to seismic activity. DEMETER is flying on a polar, nearly circular orbit at an altitude of 715 km. This orbit drifts slowly in local time, crossing the equator close to 10.30 LT on the dayside and 22.30 LT at night early in the flight. In the first part of the mission, measurements are limited to latitudes below $\sim 65^\circ$ invariant latitude. In a later stage, operations of the satellite at higher latitudes in the auroral zone and polar cap will be considered. The main objective of the ICE experiment is to measure and fully characterize the electromagnetic and electrostatic emissions in the ionosphere in order to search for signals linked to seismic events. As a secondary objective, this instrument will study man-made electromagnetic emissions that affect the particle populations in the Earth's environment and it will provide detailed observations over a wide frequency band of the electromagnetic effects that are generated by tropospheric storms in the ionosphere. To these aims, the ICE instrument on DEMETER will perform a continuous survey of the DC and AC electric fields over a wide frequency range and with a high sensitivity. The instrument and the onboard data processing have been designed to provide an optimum set of data in the various frequency ranges, emphasizing full characterization of the 3 components of the waves at frequencies below 1 kHz and single-axis waveform transmission and spectrum measurements at higher frequencies.

2. Objectives of the experiment

Previous observations from space or from ground-based receivers related to seismic activity have mainly been reported at ELF and VLF and therefore efforts will be concentrated in these two frequency ranges. In addition, propagation conditions in the atmosphere and ionosphere allow electromagnetic ELF and VLF emissions that originate from the ground or from the low altitude atmosphere to reach ionospheric levels as is the case, for example, of thunderstorm-generated whistlers which cover a wide frequency range but have their maximum energy at rather low frequencies. Beyond the simple detection and measurement of natural and man-made emissions, of particular interest is the detailed characterization of these electromagnetic waves and in particular the determination of their polarization and propagation direction or **k** vector. This can be achieved by measuring simultaneously their 3 electric and 3 magnetic components. Due to the very large corresponding data volume, it is only possible, in practice, to perform such detailed measurements in the ELF range and during dedicated *Burst modes* of operation. This is one of the central objectives of the ICE and Magnetic Search Coil Antenna (IMSC) experiments. In parallel to the 6 ELF channels, the waveform of one electric component will be transmitted in order to extend detailed observations in the VLF range, although this will not allow polarization or propagation direction determination at these frequencies. In ordinary *Survey modes* where the data rate is reduced, ICE will measure the power spectrum of one electric component over the ELF and VLF ranges.

Observations of HF wave emissions associated with seismic activity are more seldom and have been thus far reported from ground instruments only. If ducted propagation along magnetic field lines occurs with less efficiency in this frequency range than at ELF and VLF, perhaps because density gradients are more transparent to smaller wavelengths, other types of HF emissions can still be generated by local instabilities of the ionospheric plasma and need to be surveyed. The HF channel on ICE is designed to measure emissions at the plasma frequency corresponding to electron densities of about $10^5\,\mathrm{el\,cm^{-3}}$ and below. In the current period of low solar activity this is the expected plasma density range at night along the DEMETER orbit.

There are also two important secondary objectives of the DEMETER ICE instrument. These include: (1) observations of ionospheric effects above thunderstorms regions and (2) a survey of the wave activity in the Earth's environment. In the last decade and following the discovery of sprites, a number of experiments have been realized to study electrical discharges occurring above thunderstorms, to observe the related luminous structures (e.g. Sentman and Wescott, 1993) and to measure the electromagnetic emissions that are generated by these electrical processes. The VHF receiver experiment on the FORTE satellite (Jacobson et al., 1999) has produced a large observational data base on the thunderstorm electromagnetic emissions between 30 and 300 MHz (Jacobson et al., 2000). Studies conducted at lower frequencies have shown that ELF and VLF measurements may also provide insight into the cloud-to-ionosphere electrical discharges (Boccipio et al., 1995; Dowden et al., 1996). The ICE nearly continuous observations of natural emissions from ELF to HF, will therefore provide a very useful set of data in this domain and help in understanding the electromagnetic coupling between the atmosphere and the ionosphere. At night and in the current period of low solar activity, plasma densities in the E and F layers may be lower than $\sim 10^4\,\mathrm{el\,cm^{-3}}$ at mid-latitudes and hence allow HF emissions in the upper range of the ICE frequency bandwidth to propagate to the altitude of DEMETER. Other types of disturbances can also be expected in the vicinity of thunderstorms. For example, large electric fields generated in the stratosphere by the highly electrified cloud tops map to higher altitudes. Even if they are strongly attenuated due to the exponential increase of the atmospheric electrical conductivity with altitude, they can produce detectable disturbances in the electric field pattern at the base of the conductive ionosphere. Such disturbances may reach several mV/m and are ultimately transmitted to higher altitudes along the equipotential field lines. Thus, they should be detectable by instruments onboard DEMETER. Associated with the changes in the thunderstorm-related DC electric fields electrostatic turbulence can also arise (Farrell et al., 1994)

as well as plasma motion detectable by the IAP (Plasma Analyzer) experiment.

The other secondary objective of the ICE experiment is to provide a database on the electromagnetic environment of the Earth and in particular of man-made emissions, from the harmonics of power lines to VLF and HF transmitters. Knowing the characteristics of the VLF transmitter signals in the ionosphere is needed to appraise their influence on the trapped particle populations and obtain quantitative understanding of the de-trapping of the energetic electrons and their precipitation in the lower ionosphere. Other aspects of the interaction of strong VLF signals from ground transmitters with the ionospheric plasma will be studied such as the generation of side bands and the broadening of the VLF signal in relation to the ambient natural electromagnetic noise. The overall frequency range of interest extends from the low-frequency part of the ELF channels for the power lines into the VLF range and possibly also the HF range where high power transmitters may be detectable.

3. Description of the experiment

The ICE experiment consists of 4 *spherical sensors*, with embedded pre-amplifier electronics, mounted on the ends of 4 stacer booms or antenna "arms", and *associated electronics* included in the BANT module to fulfill the onboard signal-processing requirements.

3.1. ICE sensor configuration

Stacer booms similar to those used by the ICE experiments have been used on a very large number of satellite and rocket experiments to deploy electric field probes, e.g. on the FAST satellite (Ergun et al., 2001). They have a length of 4 m and are deployed as shown in Fig. 1. Sensors E_1 and E_2 are deployed parallel to the satellite Y-axis, perpendicular to the satellite XZ plane which is the orbital plane for the nominal attitude of the satellite.

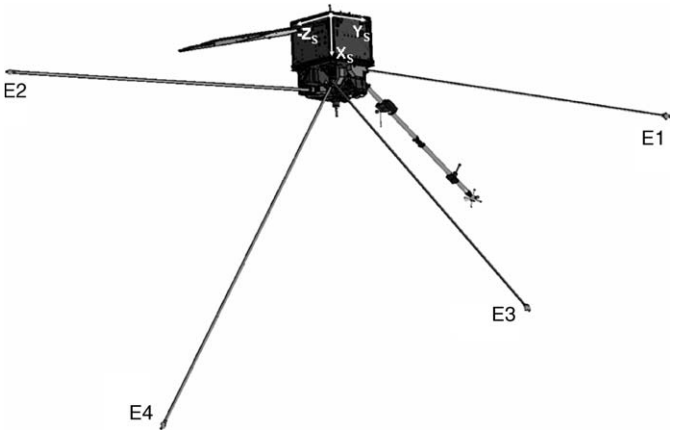

Fig. 1. ICE sensor configuration on the DEMETER satellite.

Sensors E_3 and E_4 are deployed at 45° from the X-axis, which is the nadir direction, and at distances of about 15 cm on both sides of the satellite XZ plane. In this configuration, the 3 sensors E_1, E_3 and E_4 are located at a distance of 4 m from the satellite and sensor E_2 is at a distance of the edge of about 2.3 m to the solar panel.

In the mid-latitude and equatorial ionosphere along the orbit of DEMETER, the electron density typically ranges from $\sim 10^5$ to $\sim 10^3$ el/cm^3 and the temperature from 1000 to 3000 K, corresponding to Debye lengths λ_D in the range of $\leqslant 1$ to ~ 10 cm. In the nightside auroral or polar ionosphere and in winter, the Debye length may reach 20–30 cm for cases of a highly depleted hotter ionosphere. With 10 λ_D as a reasonable estimate of the maximum extent of the plasma sheath around the satellite and its appendices, sensors E_1, E_3, and E_4 are located well outside the spacecraft plasma sheath even for unusual events and E_2 is also outside the sheath of the solar panel. All sensors are far enough from the wake produced by the spacecraft motion through the ionospheric plasma. The wake extends along the Z direction with a maximum cross section perpendicular to the Z direction of about 2 times the satellite size, thus about 1.5 m, at a distance from the satellite of about 2 m.

Special care was taken to have the external surface of the spacecraft and solar panel equipotential at spacecraft ground. This was achieved by wrapping most of the satellite surface in a conductive carbon-filled kapton MLI with only 10–15% of the surface exposed to the ambient plasma left non-conductive. In addition, the solar cell cover glasses were coated with a conductive tin oxide layer also connected to the satellite ground, leaving only the very thin connection wires between adjacent individual solar cells in contact with the plasma. Thanks to these arrangements, the disturbances of the plasma potential that could arise from the extended pre-sheath are therefore minimized and should not therefore raise any problem under practically all plasma conditions that can be encountered along the orbit of DEMETER.

When measuring the potential difference between two of these sensors, ICE operates as a double probe instrument (e.g. Mozer, 1973) in which the component of the electric field is determined along the axis defined by the two sensors. Any pair of sensors among the four can be used for this objective which enables the 3 components of the DC and AC vector electric field to be obtained. The nominal configuration of these 3 components is the following:

- E_{12} ($\approx$along the Y-axis of the spacecraft) $= E_1 - E_2$,
- E_{34} ($\approx$along the Z-axis of the spacecraft) $= E_3 - E_4$,
- $E_R = E_{13} = E_1 - E_3$.

The optimized orientation of the 4 booms thus allows to get in practice 2 components of the electric fields in the orthogonal frame of reference of the satellite axis with very

minor corrections from the other components, thus with a negligible impact on the final accuracy.

As seen from above, the E_1 and E_3 sensors are each used to measure 2 components of the electric field vectors. In order to minimize the detrimental effects that might arise should any of them fail, a telecommand order is available to replace them by, respectively E_2 or E_4 in the E_R component. Thus E_{12} and E_{34} are sent to telemetry irrespective of the sensors status and the third component E_R can be changed to E_{23} ($=E_2-E_3$) if E_1 fails or E_{14} ($=E_1-E_4$) if E_3 fails.

3.2. Sensor description

The 4 sensors are spherical aluminum electrodes 60 mm in diameter shown in Fig. 2(A). Non-uniformity of the electrode surface work function and resulting differences in the average surface potential between electrodes are two main causes of errors in DC electric field measurements. In order to minimize these effects, the spherical electrodes are coated with a carbon-filled epoxy (DAG 213 from Acheson Ind. Inc), with a minimum thickness greater than about 30 μm. Such a coating has been widely used in past space and laboratory measurements have shown rms variations of the surface potential to be on the order of ~20–40 mV. Previous in flight observations have also shown that the average contact potential differences between spherical electrodes of similar size was typically a few tens of mV. Contrary to the case of a double probe instrument on a spinning satellite where the contact potential differences between the two sensors appear as offsets on a quasi periodic signal and can be easily eliminated, such differences are more difficult to correct on a three-axis stabilized spacecraft as DEMETER. The absolute error on the large-scale quasi-DC electric field measurements would thus range from a few to 10 mV/m. A detailed statistical data analysis has to be performed to correct this error and improve the measurement. It is foreseen, in particular, to take advantage of spacecraft maneuvers when its orientation varies. Nevertheless, due to the relative stability in time of the electrode surface potentials, small-scale quasi-DC electric fields can be accurately measured as disturbances superimposed on the large scale, slowly varying signals which arise mainly from the induced $\mathbf{V}\times\mathbf{B}$ electric field. For the orbit of DEMETER and the foreseen solar activity over its 2-year operational phase, the calculated lifetime of the DAG 213 coating against chemical reaction and erosion by atomic oxygen is about 11 years. This ensures that the coating will remain practically unaffected during the whole mission. Titanium nitride (TiN) may have provided somewhat better performances (Amatucci et al., 2001) and less sensitivity to atomic oxygen. However, due to its thermo-optical properties, this coating would have resulted, on the sunlit part of the orbit, in operating temperatures in excess of 100 °C, thus too high for the electronics. With the DAG 213 coating, the operating temperature of the electronics in the ICE sensors stays in the range −25 to 40 °C.

Embedded in each spherical electrode shell, is a small electronics board consisting of a unity gain preamplifier and a polarization current source shown schematically in Fig. 2(B). The current intensity, which is the same for all 4 sensors, can be adjusted through telecommand and is used to control the impedance of the electrode sheath, mainly its resistance which is more variable than its capacitance. This is important for two reasons. First the sheath resistance must be maintained to negligible values compared to the input impedance of the pre-amplifier, in order to guarantee the accuracy of the amplitude of the quasi-DC and low-frequency electric field measurements. In addition, the sheath resistance varies along the orbit as a function of the electron density and temperature and in nighttime low-density plasmas non-polarized electrodes at floating potential may have sheath resistances in excess of 10 MΩ. Such high values induce large-frequency-dependent attenuation and phase shifts of the measured electric components which should be taken into account when determining the propagation vector $\mathbf{k}$ of electromagnetic waves when using simultaneous measurements of the ELF electric and magnetic components. To avoid such a complicated and unavoidably inaccurate real time, dynamic correction, the solution is to maintain the sheath resistance at low enough values for all expected plasma conditions in order that no correction of the measured electric components is needed at first order up to the ~1 kHz frequency limit of the ELF channel. This can be achieved by using a large enough polarization electron current which will bring the potential of the electrode closer to plasma potential and reduce the extent of the sheath and its impedance.

In order to help determine the necessary polarization current, the impedance of two electrodes, S_1 and S_3, are measured during short calibration sequences which are run at the beginning of each *Burst* (1 s duration) and *Survey modes* (4 s duration) and also, nominally, every 4 min inside a mode. To this aim, two AC low amplitude modulations at 625 Hz and 10 kHz are superimposed on the DC polarization current of these two electrodes. The resulting modulations of the potential of the two sensors are readily detected on the E_{12} and E_{34} signals in the ELF and VLF channels, from which one can compute the sheath impedance and check the adequacy of the polarization current. In addition, it is foreseen to build a database of the sheath impedances and plasma parameters (Ne and Te) obtained from the ISL data, to retrieve the sheath impedance from any measured values of Ne and Te. This database can be used, if necessary, during high-level data analysis to perform fine corrections of the electric components before computing the propagation characteristics of the ELF electromagnetic waves.

Electronic circuits inside the sensors are housed in a double shield with its internal part at ground potential and the external shield, bootstrapped at the preamplifier output

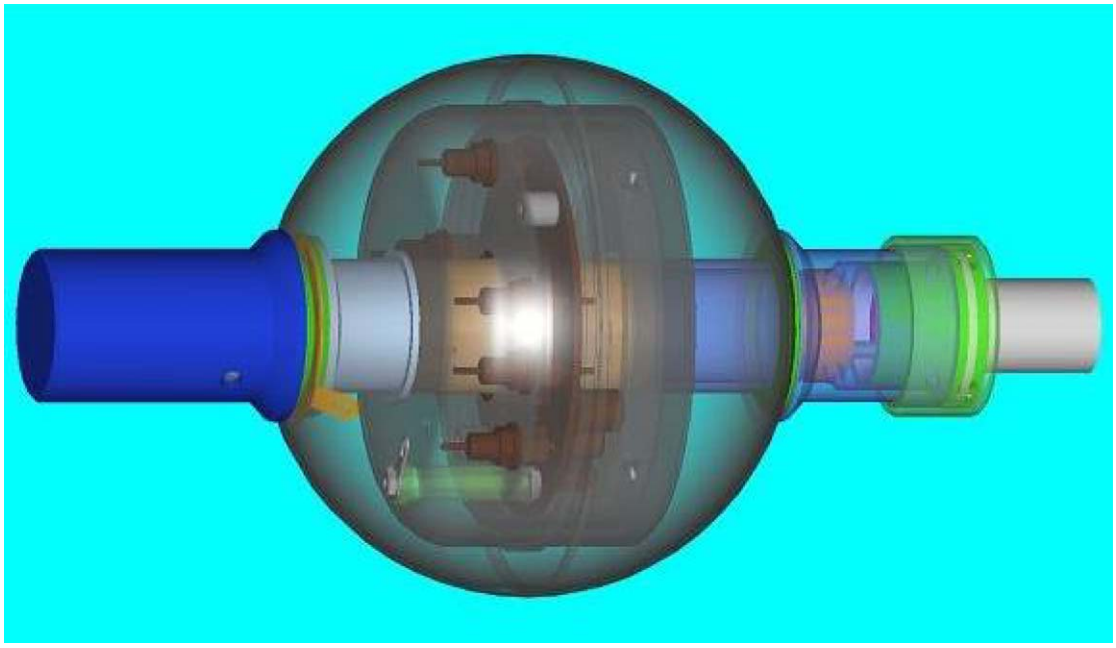

(A)

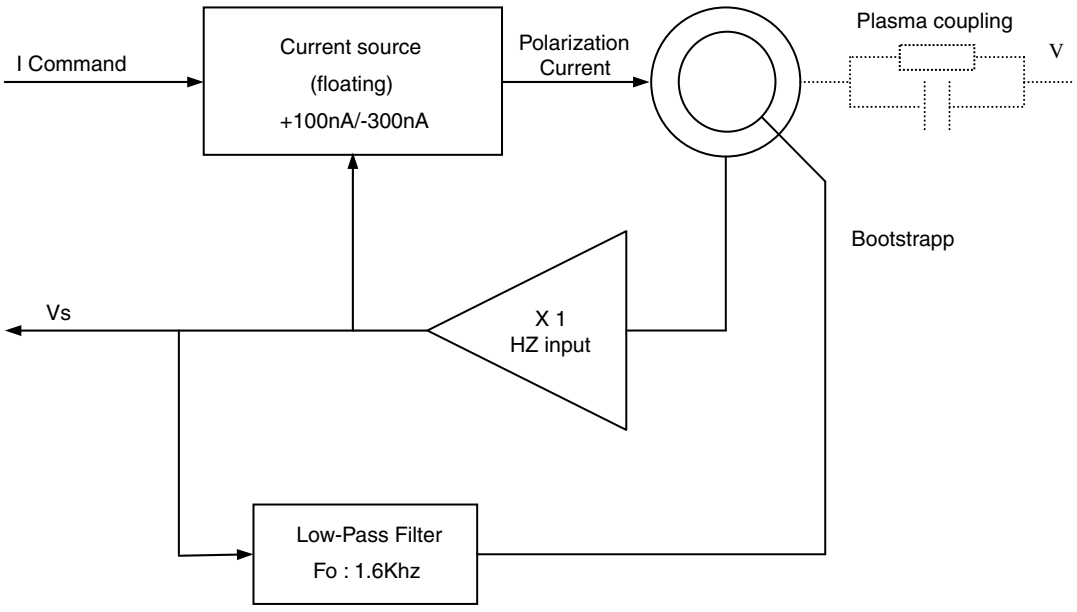

(B)

Fig. 2. (A) The ICE electric field sensor. The sphere has been represented as transparent to show the embedded electronics and housing. (B) The ICE electric field sensor electronics.

voltage, thus at the sensor potential itself. This set-up minimizes the parasitic capacitance in parallel to the preamplifier input and improves the frequency response of the polarization current generator which is effective up to ~2 kHz.

The sphere is mounted at the end of the boom through a cylindrical stub (Stub 1), 4 cm in length, which is used as the interface between the sensor and the boom. The external surface of this stub is coated with the same coating as the sphere. Diametrically opposite is an identical stub (Stub 2) also with the same coating. The external surfaces of the two stubs are bootstrapped at the sphere potential. These bootstrapped stubs insure a better quality of measurements for two reasons. First stub 1, at sphere potential, acts as a guard that prevents disturbances of the sphere potential, close to plasma potential, from the boom which is connected to the satellite ground. In addition, since stub 2 is diametrically opposite to stub 1, all 4 sensors are made symmetrical at first order to effects arising either from the shadow or from the wake of the boom projected onto the sphere or from the effect of the ambient magnetic field. This minimizes all disturbing effects and improves the

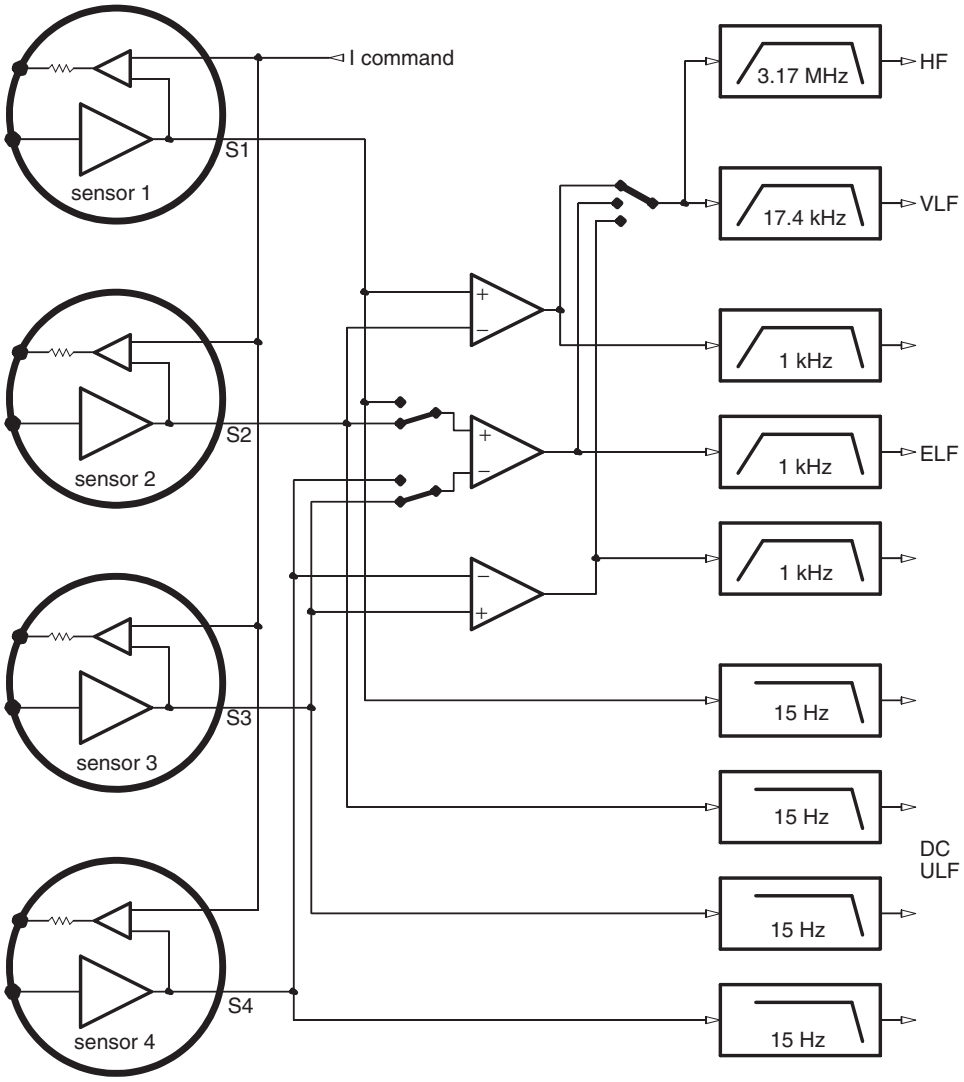

Fig. 3. ICE electronics block-diagram.

quality and accuracy of electric field measurements, in particular in the DC and ELF range.

3.3. On board signal processing and electronics

The ICE electronics block-diagram is shown in Fig. 3. The electronics, included in the BANT module, encompasses an analog part with a set of filters and amplifiers to process the analog signals from the sensors and a digital part to carry out the waveform digitization, power spectra computation, and telemetry interfaces. This electronics is described in more details by Parrot et al. (2005) and will be briefly reviewed here to provide the necessary understanding of the data acquired by the ICE experiment.

Four frequency ranges have been selected, providing a set of analog signals subsequently directed to the data digitization and processing unit. Depending on the frequency range, on the spacecraft mode of operation (*Burst or Survey*), and on the ICE modes of operation, the data that are stored in the mass memory and subsequently transmitted to ground are either *waveform* data or/and *power spectra*. A description of the ICE frequency channels is provided below.

3.3.1. DC/ULF (0–15 Hz)

Four channels of waveform data for the potentials of the 4 electrodes, E_1, E_2, E_3, E_4. The signals are sampled at 39.0625 Hz and digitized with 16 bits, with a corresponding resolution of ~0.3 mV for potential measurements equivalent to ~40 μV/m for electric field measurements. DC and ULF data of all 4 sensors are available in all modes of operation.

3.3.2. ELF (15 Hz–1 kHz)

Three channels of waveform data for E_{12}, E_{34} and E_R (*nominally E_{13}*). The signals are sampled at 2.5 kHz and digitized with 16 bits. ELF data are only available in *Burst* modes.

3.3.3. VLF (15 Hz–17.4 kHz)

One channel of waveform or spectral data for one of the components E_{12}, E_{34} or E_R. The signal is sampled at 40 kHz and digitized with 16 bits. In *Burst* modes, in parallel to the acquisition of the waveform data, their power spectrum is computed by the BANT module with a 19.53 Hz frequency resolution. 40 spectra are averaged, providing a temporal resolution of 2.048 s, and telemetered to the ground with 8-bit resolution after normalization with respect to the greatest power spectral density. The power spectrum is mainly used for Quick Look purposes. When the RNF (neural network) experiment is activated, data are analyzed by a neural network to detect the occurrence and characteristics of whistler emissions from thunderstorms.

In *Survey* modes, only the power spectrum is stored in the mass memory and there are 3 ICE sub-modes. In the first one, labeled (0), the frequency and temporal resolutions are identical to those of the Burst mode, in the second one (1) the temporal resolution is increased to 0.512 s and in the third one (3) the frequency resolution is decreased to 78.125 Hz by averaging over 4 consecutive frequencies.

3.3.4. HF (10 kHz–3.175 MHz)

One channel among E_{12}, E_{34} and E_R, the same as in the VLF range. The signal is sampled at 6.66 MHz and digitized with 8 bits. The HF data acquisition is performed on 40 data snapshots each 0.6144 ms long and evenly spaced in the 2.048 s elementary interval of the VLF channel acquisition. Individual power spectra are calculated for each snapshot with a frequency resolution of 3.25 kHz and averaged to provide a power spectrum every 2.048 s.

In *Burst* modes, the averaged power spectrum and waveform data for a single 0.6144 ms interval are available. Through a telecommand order, the selected waveform interval can be either the first of the 40 intervals or the one with the maximum total power over the entire HF bandwidth.

In *Survey* modes, the power spectra are the only information available and there are 3 sub-modes similar to those in the VLF Survey mode, with varied frequency and temporal resolution: (0) and (1) provide a 3.25 kHz frequency resolution with, respectively a 2.048 s (average over 40 spectra) and 0.512 s (average over 10 spectra) temporal resolution, while (2) provides a 13 kHz frequency resolution (averaging over 4 consecutive frequencies) and 2.048 s temporal resolution.

4. In-flight performances

4.1. Noise level and interferences with other instruments

In Fig. 4 are displayed the in-flight noise power spectra of the ICE experiment for the E_{12} electric field component in 3 frequency ranges, ULF/ELF (panel a), VLF (panel b), HF (panel c). In order to evaluate the true noise level of the instrument, quiet periods with ideally no or, in practice, as weak as possible, natural emissions must be found. Two different intervals of time have been used, one on a dayside pass in orbit 821 at ELF and the other one on a dayside pass in orbit 806 at VLF. In each case 40 individual spectra computed on elementary blocks of 51 ms of data have been averaged. In these two frequency ranges the noise is identical for day and night passes. In the HF range, the noise is markedly different for day and night passes because of the influence of the solar panels and associated electronics. Therefore two passes have been selected, one on the dayside (orbit 3155), the second one on the night side (orbit 3117). In each case 17 spectra computed on 0.6144 ms elementary intervals of time were averaged to produce the plot. The average noise level is about $0.1\,\mu Vm^{-1}\,Hz^{-1/2}$ above 100 Hz in the ELF channel, $\sim 0.05\,\mu Vm^{-1}\,Hz^{-1/2}$ in most of the VLF range and $\sim 0.1\,\mu Vm^{-1}\,Hz^{-1/2}$ over the HF range. The average ELF noise level is thus at least 20 db below the values quoted by Molchanov et al. (1995) for ELF waves possibly related to earthquakes and also well below the typical intensities of natural emissions of ionospheric and magnetospheric origins observed at low altitudes such as plasmaspheric hiss ($0.3–3\,\mu V\,m^{-1}\,Hz^{-1/2}$), whistler-mode and Z-mode auroral emissions ($10–100\,\mu V\,m^{-1}\,Hz^{-1/2}$), ELF electrostatic equatorial turbulence ($1–3\,\mu V\,m^{-1}\,Hz^{-1/2}$) and ELF electrostatic auroral turbulence ($3–30\,mV\,m^{-1}\,Hz^{-1/2}$). In the ELF range there are a number of discrete frequency lines, at 7.33, 19.53, 39.06 Hz and their harmonics, with intensities below $\sim 1\,\mu Vm^{-1}\,Hz^{-1/2}$. They are caused by interference with the digital circuits in the BANT processing electronics. Their level is very weak compared to the 80 dB dynamic range of this channel and due to their very stable frequency they can be easily eliminated if necessary and thus have no influence on the performance of the instrument. In the VLF range, there is a single parasitic line, again with a very small amplitude and insignificant with respect to the 85 dB dynamic range of this channel. In the HF range, a nearly constant, essentially instrumental noise is observed throughout the whole frequency range, with a faint maximum of $\sim 0.1\,\mu Vm^{-1}\,Hz^{-1/2}$ near 500 kHz. Superimposed on it are three groups of parasitic lines. The first one corresponds to a fundamental frequency of 91.4 kHz and its harmonics, the second one to a fundamental frequency of 119 kHz and its harmonics, the third one to a fundamental frequency of 416 kHz and its harmonics. These parasitic lines have a small intensity of $\sim 1\,\mu Vm^{-1}\,Hz^{-1/2}$ during night time passes but are amplified to $\sim 2\,\mu Vm^{-1}\,Hz^{-1/2}$ on the dayside (panel c). The first group of lines arise from the DC/DC power converter and regulator associated with the solar generator and the satellite power system, the source of the two other groups have not been identified but appear to come from the digital circuits of the BANT module since they are mainly observed in *Burst modes*. However, even the dayside levels are small enough not to hamper the dynamic range of the HF channel equal to ~42 dB. In addition, all these frequencies are very stable and, if necessary, the parasitic

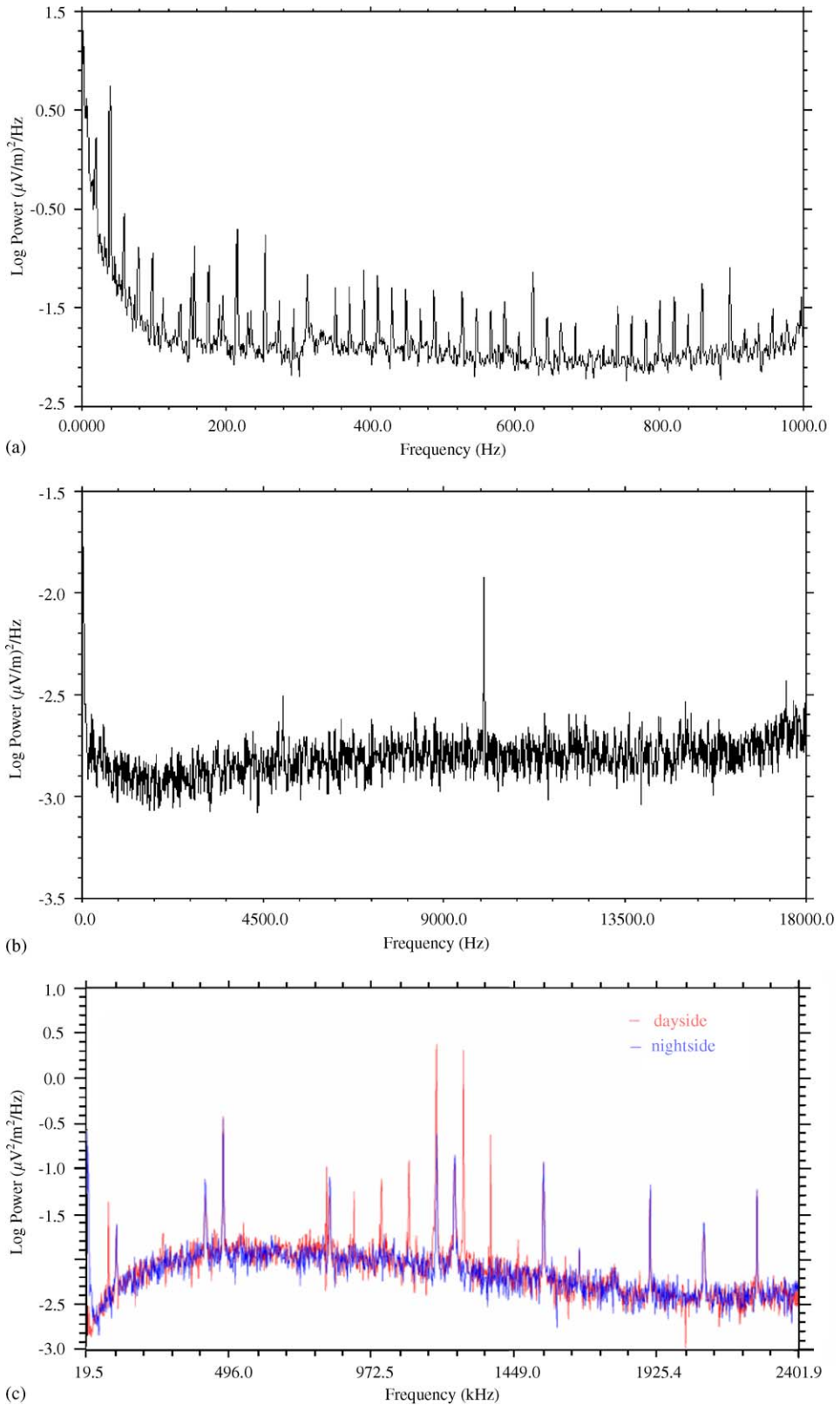

Fig. 4. In-flight noise levels of the ICE experiment: (a) ULF-ELF channel; (b) VLF channel; (c) HF channel.

lines can be easily removed from the signal during ground processing. Fig. 5 provides an overview of the sensitivity level of the experiment over its entire frequency range, from DC to 3.175 MHz.

The ISL (Langmuir probe) instrument, located on the boom that holds the magnetic antennas (see its position on Fig. 1), is the only experiment in the scientific payload that generates a noticeable level of interference on the ICE data.

These interferences result from the sweep voltage applied to the ISL Langmuir probes (Lebreton et al., 2005). The amplitude of this sweep is fairly large, ranging originally from −7.6 to 7.6 V in the nominal mode of operation, and

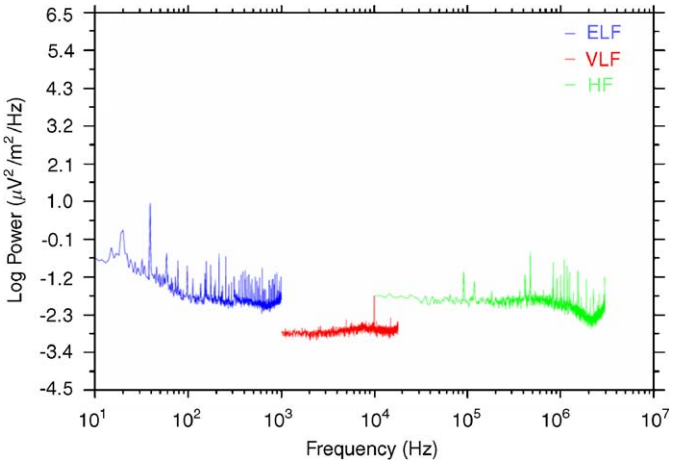

Fig. 5. Overall sensitivity curve for the entire frequency range from DC to 3.175 MHz.

results into two main effects. In practice, the first one is observed only when the largest ISL probe, the segmented Langmuir probe (SLP), collects an electron current. When the electron current collected by the SLP probe increases, the satellite potential has to become more negative to insure that the ion current collected by the satellite stays equal to the electron current collected by the probe. To first order, in an oxygen plasma, the ratio of the ion current to the electron current is about 1/170. Since the effective collecting surface of the satellite and solar panel is only about 300 times larger than the area of the probe, the change in the satellite potential is therefore appreciable and readily seen on the direct measurements of the ICE probe potentials in the ULF channel. This disturbance cancels when one performs differential measurements to obtain the electric field which is the case for the higher frequency channels. The second effect stems from the fact that both probes of the ISL experiment act as antennas in the plasma during the fast fly back of their swept voltage and transmit a parasitic emission with a wide enough spectrum which can be detected by ICE in the ELF and VLF ranges. This effect appears to maximize close to the equator and thus

Table 1

Current (nA)	0	−40	−80	−100	−120	−150	−180	−200
Ne (el/cm^3)	4×10^3	7×10^3	3×10^4	10^4	3.5×10^3	1×110^4	3×10^4	1.2×10^4
Model R_s	5.8 MΩ	1.45 MΩ	415 kΩ	580 kΩ	480 kΩ	385 kΩ	325 kΩ	290 kΩ
R_s	1.5 MΩ	940 kΩ	320 kΩ	570 kΩ	1.18 MΩ	430 kΩ	245 kΩ	380 kΩ
C_s (pF)	3.6	3.85	4.8	5.3	3	4.5	4.45	4.6

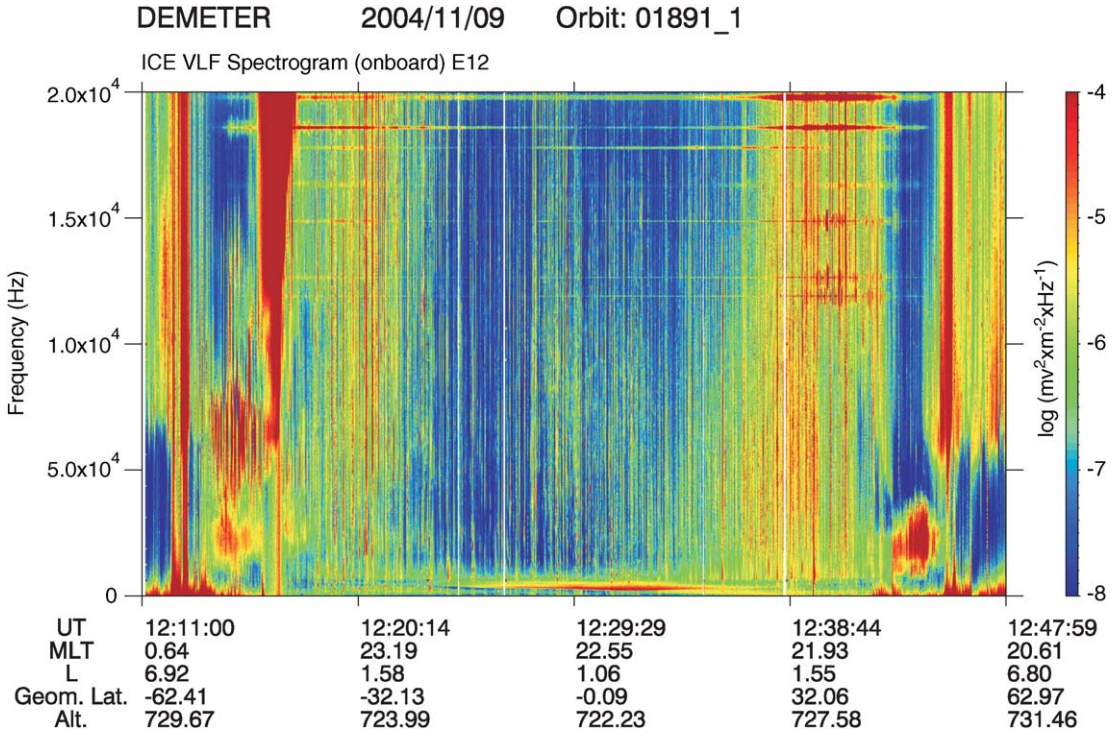

Fig. 6. Example of a nighttime pass showing plasmaspheric hiss, lightning emissions and VLF transmitters at mid latitudes and electrostatic turbulence in the auroral regions.

for a rather specific orientation of the satellite with respect to the magnetic field (D. Lagoutte, unpublished document). This phenomenon is presently under study. Interferences of this kind have been noticeably reduced by modifying the ISL voltage sweep from −3.8 to 3.8 V.

4.2. Sensor sheath impedance

As explained above, the sheath impedance is determined by modulating the polarization current of two sensors E_1 and E_3 at two frequencies 625 Hz and 10 kHz with an equal amplitude $i_m = 33$ nA. The output signals of channels E_{12} and E_{34} are a direct measurement of the voltage V_m induced by these AC currents through the sheath impedance. A straightforward calculation provides the resistance R_s and capacitance C_s of the sheath. Measurements shown in Table 1 were made early in the flight during the nighttime portion of orbit 196 during 3 sequences about 1 min long each with the sensors polarized with a DC electron (i.e. negative) current which was varied over 8 steps from 0 to −200 nA. Since the ISL experiment was still not activated during this test orbit, an initial analysis of the data have been made using the preliminary ion density provided by the Plasma Analyzer (IAP), with an accuracy of $\sim\pm 20\%$ and assuming an electron temperature of 2000 °K. Displayed in Table 1 are some values of R_s and C_s obtained in the nighttime mid-latitude and equatorial ionosphere on the ascending part of orbit 196. They were compared to a simple estimate of the probe resistance, kT_e/eI, where I is the current collected by the probe. This approach is only valid when all other currents to the probe (essentially the ion current and the photoelectron current) can be neglected compared to the thermal electron current.

Uncertainties in the computed values of sheath resistance and capacitance indicated in Table 1 are typically ~10–15%. The main source of error in the modelled sheath resistance is the assumed value of 2000 K for the electron temperature since current observations by ISL vary over a relatively wide range, from 1500 to 3500 K. Except at low plasma densities, i.e. below $\sim 5 \times 10^3$ el cm^{-3}, the measured values and those deduced from the simple model are in quite good agreement, with deviations less than ~20%. As expected the sheath resistance varies approximately as the reciprocal of the polarization current. Polarization electron currents of about 80 nA and above provide sheath impedances small enough not to require a significant correction of the measured electric fields in the ELF range up to 1 kHz.

5. Initial observations

In order to briefly illustrate the measuring capabilities of the instrument we have assembled in this last section some typical examples of data that were acquired during the first months in orbit.

5.1. Plasmaspheric hiss and VLF transmitters

Fig. 6, corresponding to the night part of orbit 1891 on 9 November 2004, provides an overview of typical night time ELF and VLF electric fields measurements. The main source of natural emissions is the auroral and plasmaspheric hiss. Plasmaspheric hiss is clearly visible in the low latitude part of the orbit with a sharp cut-off which follows the H^+ gyrofrequency. At higher latitudes, structured VLF emissions dominate in two frequency ranges, from 2 to 3 kHz and above 6 kHz, extending above 20 kHz, the frequency limit of the VLF channel. At mid-latitudes the most intense and regular sources are the lightning generated whistler emissions clearly visible on the figure in particular around 12:38 UT at a latitude of ~30°. In the auroral zone, several structured bursts of electrostatic turbulence occur both in the northern and in the southern hemisphere, extending up to ~1 kHz. Gradient drift instability driven by the fast auroral plasma convection (e.g., Cerisier et al., 1985) or instabilities generated by field-aligned currents are likely mechanisms to produce these bursts of electrostatic turbulence. Some of them are associated with intensifications of the signals that extend over the entire frequency range and are probably related to plasma density structures that act as ducts for ELF and VLF whistler waves as shown by Beghin et al. (1985).

In addition to the natural emissions, a number of isolated VLF frequency lines are clearly visible above 12 kHz that are due to the propagation in the upper ionosphere of the electromagnetic waves from radio-navigation VLF transmitters. They are observed at frequencies above 10 kHz on either sides of the equator and their occurrence and intensity show significant day to day variations that are in particular associated with the magnetic activity. A number of interesting features, in particular above ~18 kHz, can be observed revealing a rich variety of interactions with the ambient ionospheric plasma and with natural waves: generation of side lines either on both sides or on a single side of the central frequency, broadening of the power spectra in the region of occurrence of lightning generated whistlers, etc. A discussion of these observations is outside the scope of the present paper and will be reported in a forthcoming publication.

5.2. Frequency modulation of VLF emissions

Whistler-mode VLF emissions with intensity modulated at frequencies in the ULF range are commonly observed both on the ground and on board satellites within the magnetosphere. Over the last decades, numerous studies have been devoted to their seasonal, diurnal, and latitudinal variations in occurrence, their association with geomagnetic micropulsations or not, and the mechanisms leading to their generation (Helliwell, 1965; Sato and Kokobun, 1981; Sato and Fukunishi, 1981; Sazhin and Hayakawa, 1994; Smith et al., 1998; Engebretson et al.,

2004). Emissions with modulation periods below 10 s, including whistler-mode waves propagating along magnetic field lines and echoing between opposite hemispheres, hisslers and pulsing hiss, are often termed as periodic emissions (PEs). Emissions with periods over 10 s, known as quasi-periodic emissions (QPs) are usually classified into two types, QP1 and QP2, according to whether emissions are closely associated with geomagnetic pulsations of the same period as that of the modulation or not. However, this distinction between QP1 and QP2 is based on ground observations and is not always obvious when considering QP emissions observed on board satellites. The close association between QP1s and geomagnetic pulsations is usually interpreted as the result of the modulation of the VLF whistler-mode cyclotron instability growth rate by Pc3-4 geomagnetic pulsations.

Observation of QP emissions is of common occurrence in DEMETER data. Most of the time, these emissions are observed at middle latitudes and sub-auroral latitudes and appear as rising tone structures in the frequency–time spectrograms with modulation periods ranging from ~ 20 s to more than 1 min. QP emissions observed at low latitudes occur at frequencies just above the lower cut-off of plasmaspheric hiss at the proton gyrofrequency. Two different types can be distinguished, as illustrated by the electric spectrograms of ELF and VLF waves recorded at equatorial latitudes (L$\sim$1.05–1.2) displayed in Fig. 7. The first one (upper panel) is similar to that observed at higher latitudes and consists of discrete elements with rising frequency over a frequency band of a few hundred Hz and with a modulation period of $\sim$120 s. The second one (bottom panel) shows an example of more complex QP emissions that have been observed during the recovery phase of an intense geomagnetic storm (Dst ~ -300 nT). In this figure is clearly seen the continuous cut-off frequency close to the H+ gyrofrequency with a minimum at the equator. Also, north and south from a $\sim 15^\circ$ wide equatorial region, waves are seen to propagate below this cut-off down to the bi-ion cut-off frequency (Gurnett and Burns, 1968). Emissions consist of a combination of two rising tone structures observed simultaneously, the first in the frequency range 400–900 Hz just above the proton gyrofrequency and characterized by a modulation period of $\sim$10 s, the latter from $\sim$900 Hz up to 1.7 kHz, less intense and with a longer modulation period $\sim$30–35 s. Some elements of the second structure appear as the continuation in frequency of elements belonging to the low-frequency structure, which seemingly indicate that both structures are linked to the same generation process. Although it is likely that magnetic pulsations are the driver of the observed modulations of VLF waves, it is beyond the scope of this paper to discuss the possible generation mechanism(s). A future detailed statistical study of QP events recorded by DEMETER, in combination with ground-based ULF wave measurements, should provide additional interesting information with which to test the models proposed so far.

5.3. Electrostatic turbulence at the equator

Spread F is a well-known phenomenon in the equatorial ionosphere that has drawn considerable attention for more than 40 years. Ground-based studies, mainly based on radar techniques but also complemented by rocket measurements, have been essential in providing extensive observations of the extent, structure, and dynamics of the associated ionospheric plasma irregularities, at altitudes above a few hundreds of kilometres (e.g. Kelley et al., 1982; LaBelle and Kelley, 1986). Satellite measurements (e.g., Tsunoda et al., 1982; Kil and Heelis, 1998) that sample the upper F-region above 500 km have exemplified the association of small-scale plasma instabilities with larger-scale features such as deep plasma depletion extending over an entire magnetic flux tubes. As an example of the initial measurements of the ICE instrument we have represented in Fig. 8 (top panel), observations of AC electric fields made on orbit 1103 on 16 September 2004 along the E34 axis, therefore practically in the orbital plane and along the north–south direction. They were obtained during a nighttime equatorial pass at a local time of 22:30. Strong signals appear over the ELF range under the form of successive bursts of electrostatic turbulence with typical duration from 5 to 30 s. The maximum intensity of the signal reaches a few $\mu Vm^{-1} Hz^{-1/2}$ at low frequencies with significant amplitudes up to 300 Hz and detectable signals up to the upper frequencies of the ELF channel. The horizontal distances corresponding to the duration of the individual bursts range from $\sim$30 to $\sim$200 km but, when interpreted in terms of plasma structures elongated along the magnetic field, they correspond to typical dimensions of the order of about 1–10 km perpendicular to the magnetic field lines. As shown by previous satellite and rocket observations and illustrated by the electron density (second panel from top) inferred from the ISL Langmuir probe experiment (Lebreton et al., 2005), this electrostatic turbulence originates from the crossing by the satellite of plasma irregularities with typical scale from a few meters to a few hundreds of metres. Shown in the bottom two panels are the ion densities and temperature, respectively, determined using data from the IAP thermal plasma analyzer (Berthelier et al., 2005). The density of the dominant oxygen ion O^+ and of the minor H^+ ion, displays fast variations along the orbit that are observed simultaneously with the detection of a strong electrostatic turbulence. Variations are also present in the ion temperature that, on the average, display an anti-correlation with the density variations, a lower temperature being associated with a higher density.

5.4. HF emissions

As indicated earlier, the operation of the satellite has been restricted since the launch to latitudes below about 65° invariant latitude, which most of the time dismisses the possibility of observing the intense HF wave emissions that

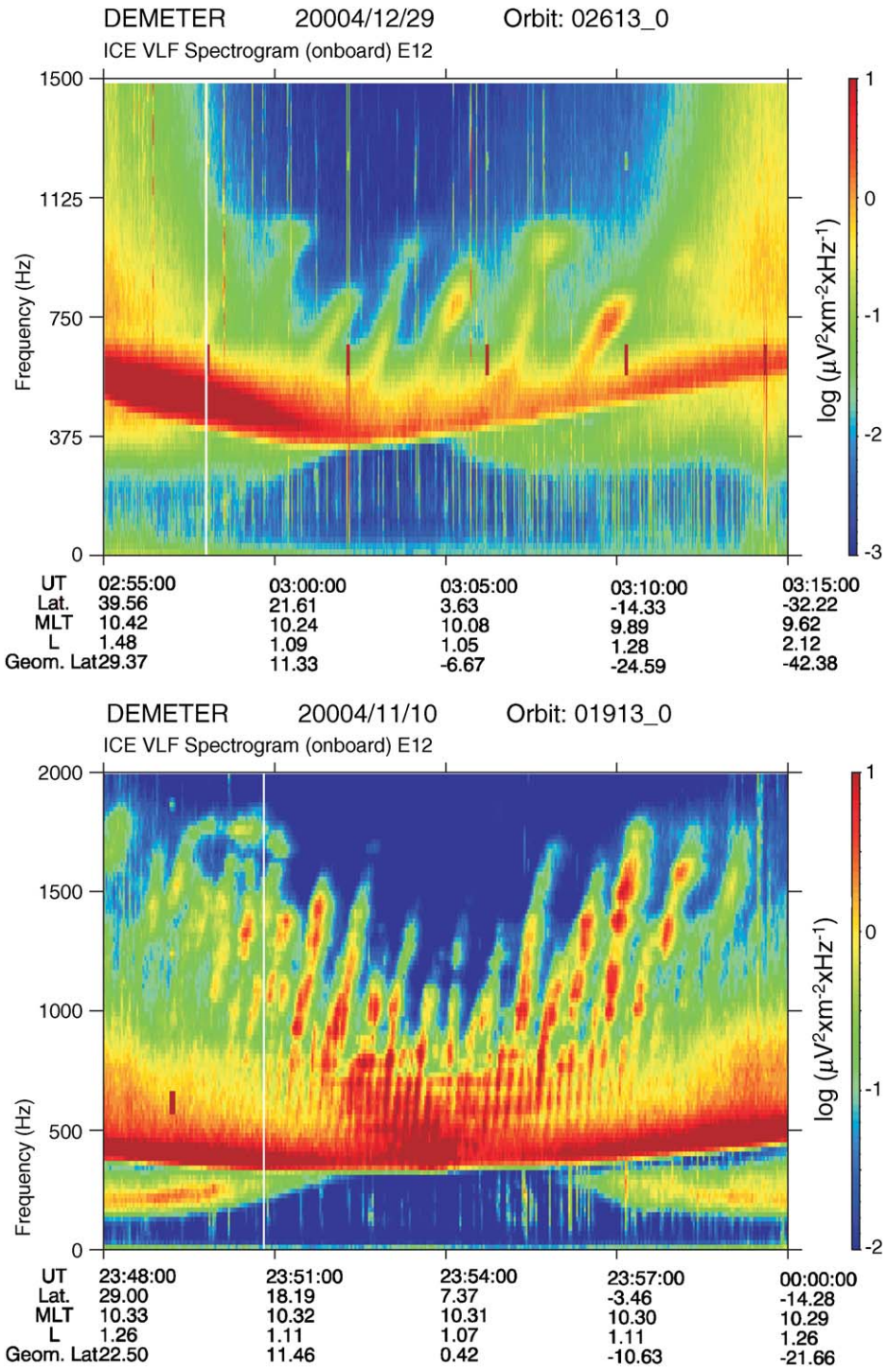

Fig. 7. Examples of quasi-periodic VLF emissions observed in the equatorial ionosphere, upper panel dayside part of orbit 2613, lower panel dayside part of orbit 1913.

occur mainly in the auroral regions (see the review by Labelle and Treumann, 2002). Nevertheless, a number of HF events have been detected with several typical characteristic spectra, especially on the evening side at subauroral and auroral latitudes just poleward of the mid-latitude trough and near the equatorial edge of the auroral oval. Fig. 9 shows an example of HF emissions (top panel) recorded during orbit 856 on 30 August 2004 in the evening MLT sector. Also displayed on the same figure are the power spectrum of the same electric component in the VLF frequency band (middle panel) and the electron density measured by the Langmuir probe experiment (bottom panel). The satellite was moving poleward, crossing the mid-latitude trough at 08:34:28 UT. The poleward edge of this trough coincides with the detection of wideband wave activity in a frequency range extending up to

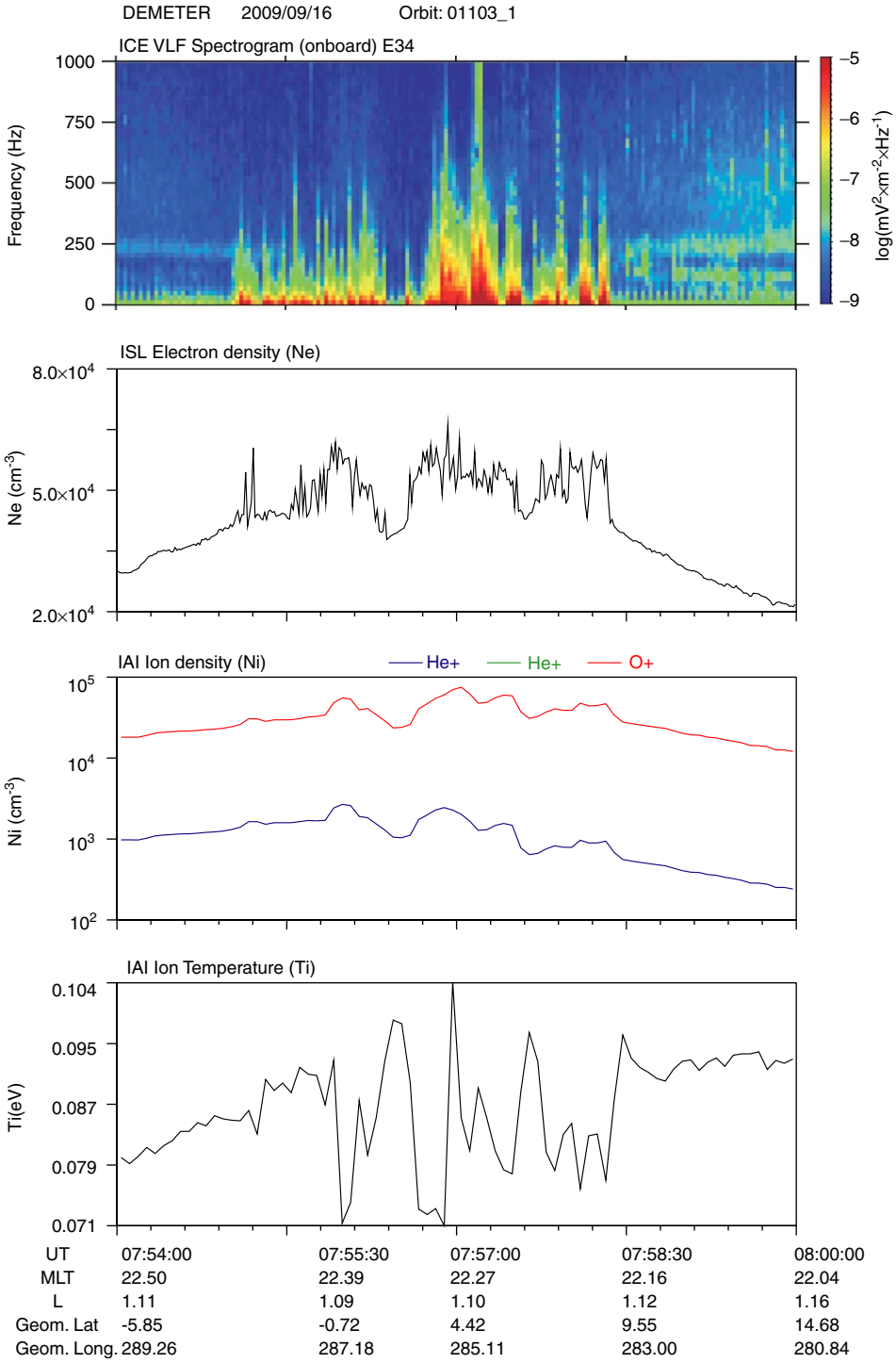

Fig. 8. Electrostatic plasma turbulence in the equatorial ionosphere and simultaneous observations of plasma irregularities. Electrostatic turbulence is shown in the upper panel, the electron and ion densities variations are shown in the two panels in the centre and the ion temperature is shown in the bottom panel.

~500–700 kHz and associated with a region of enhanced ionisation. According to values of the electron plasma frequency, f_{pe}, deduced from the electron density data and an electron gyrofrequency f_{ce} of 1.1 MHz, the low-frequency cutoff of the Z mode, $f_{L=0}$, lies between 0.59 and 1.14 MHz and the lower hybrid frequency (assuming an O^+ dominated plasma) f_{LH} near 5 kHz, which indicates clearly that the observed broadband noise consists of hiss emissions in the whistler mode. As commonly observed, the power spectral density maximizes just above f_{LH} and decreases with frequency. As the satellite enters the auroral zone, hiss emissions occur in a lower-frequency range and

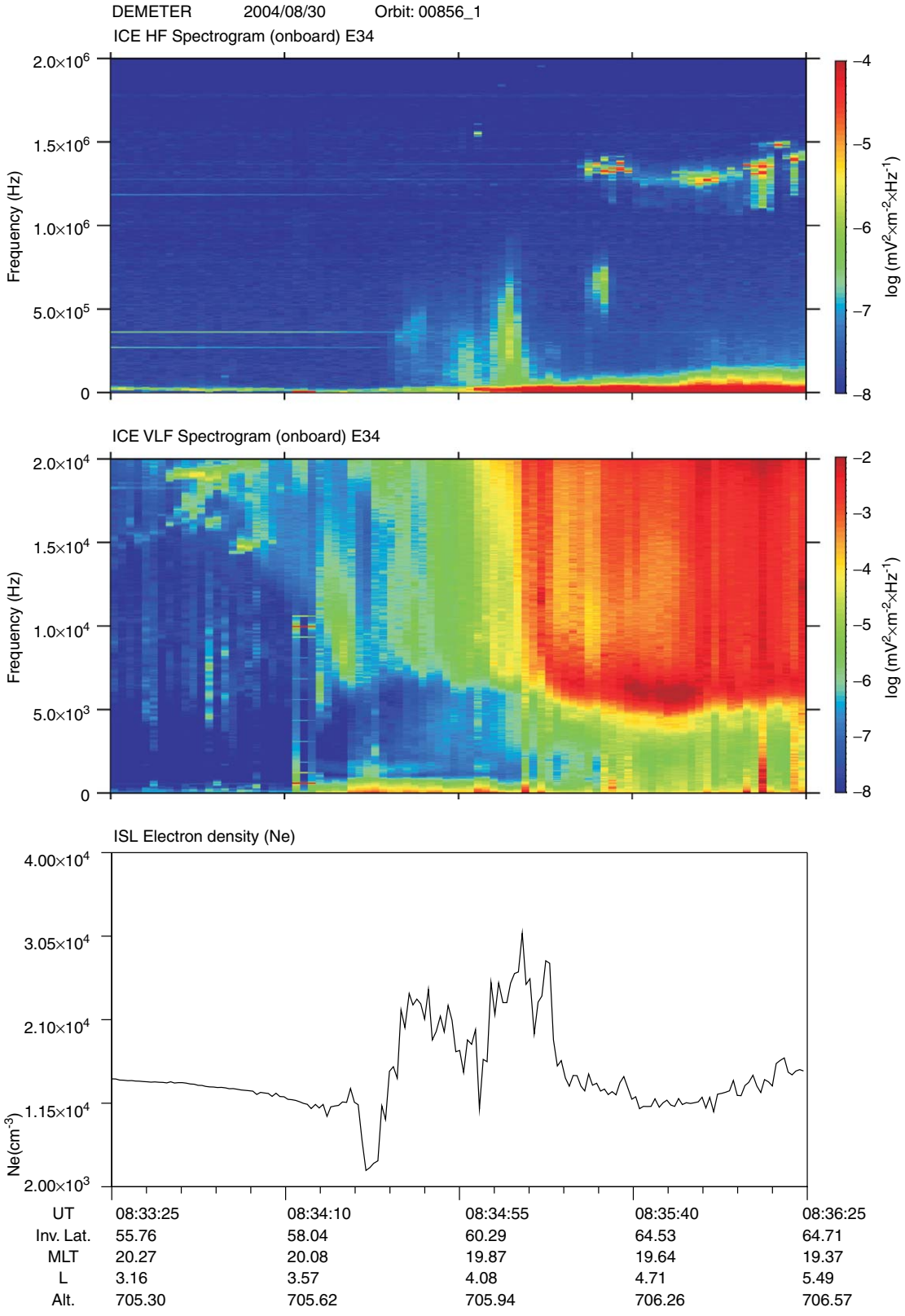

Fig. 9. Frequency–time spectrograms of one electric component of HF (top panel) and VLF (middle panel) waves recorded at sub-auroral and auroral latitudes on orbit 856 (top panel). The bottom panel shows the electron density measurements from the ISL experiment.

are much more intense with power spectral density of the order of $\sim 10^4\,\mu V^2 m^{-2}\,Hz^{-1}$ just above f_{LH}. Besides broadband VLF and LF hiss emissions, intense Z-mode emissions are observed between f_{pe} and the upper hybrid frequency f_{UH}, as the satellite enters the auroral zone (time interval 08:35:30 UT-08:36:25 UT). The frequency

evolution of these emissions follows the variation of the electron density (bottom panel). Emissions near f_{UH} dominate the spectrum with power spectral density of $\sim 10^2\,\mu V^2\,m^{-2}\,Hz^{-1}$. At these times the E34 electric antenna is at large angles with respect to the static magnetic field (80°) and therefore close to the **k**-resonance cone direction for waves in the slow Z-mode at frequencies just below f_{UH}. This may explain the spectral discreteness of these Z-mode emissions, the antenna orientation being not adequate to measure the wave electric fields at lower frequencies near f_{pe}. These emissions, often referred to as upper hybrid waves, are generated locally or nearby since they are quasi-electrostatic in nature and therefore do not propagate far from their sources. They exhibit fast amplitude variations, occur in discrete bursts of a few seconds of duration (transverse scale of a few tens of kilometers) and are often associated with an intense ELF turbulence (for instance around 08:36:13 UT), which clearly reflects the crossing by the satellite of electric current and electron precipitation structures. Because of the lack of hot plasma measurements, we cannot identify the source of free energy, probably a positive perpendicular velocity gradient in the electron distribution function (Lotko and Maggs, 1981). A third type of emissions is detected near the sharp latitudinal density gradient around 08:35:31 UT at frequencies between 0.45 and 0.75 MHz. At these times $f_L \sim 0.65$ MHz and hence they are likely whistler mode waves, even if we cannot completely rule out a mixing of whistler and Z-modes for the part above f_L. When f_{pe} is slightly larger than f_{ce}, electromagnetic whistler mode waves may be generated in the observed frequency band by loss cone or a $\partial F/\partial v_\perp$ feature in the electron distribution function via the cyclotron resonance (Wu et al., 1983). Non-locally generated whistler mode waves ducted in a magnetic-field aligned density trough might also provide another explanation, as suggested by the electron density variations measured at the same times.

6. Conclusion

The ICE experiment which presently flies onboard DEMETER has been developed to measure the 3 electric components of electromagnetic and electrostatic waves from DC to 3.25 MHz. The first objective of this experiment is to provide high sensitivity observations of electromagnetic waves that may arise from seismic activity over a wide frequency spectrum. The instrument will also be used to study man-made emissions that may affect the dynamics and life-time of energetic particles in the magnetosphere and to provide a complete database of natural emissions and plasma waves that will support on going studies in the frame of space weather programs.

The experiment uses 4 sensors, each with an embedded preamplifier and a current polarization electronics, which are deployed by 4 m long stacer booms. The geometrical arrangement has been optimised to allow accurate measurements of 3 orthogonal components of the DC and AC electric fields. The signal-processing electronics provide measurements of the sensor potentials in the ULF frequency range from DC to 15 Hz, 3 electric field components along each axis defined by the sensor geometry in the ELF range (15 Hz–1 kHz) during burst modes and, during all modes of operation, the electric field in VLF (15 Hz–17.4 kHz) and HF (10 kHz–3.175 MHz) on one of the sensor axes that can be selected by telecommand.

Boom deployment occurred early in July 2004 and the commissioning phase ended practically 2 months later. Since then, the instrument has been operated practically continuously with perfectly nominal and constant performances. The sensitivity is better than $\sim 0.1\,\mu Vm^{-1}\,Hz^{-1/2}$ above ~100 Hz in the ELF range and $\sim 0.05\,\mu Vm^{-1}\,Hz^{-1/2}$ at VLF and better than $\sim 0.1\,\mu Vm^{-1}\,Hz^{-1/2}$ in the HF range. Based on the set of earlier observations, these sensitivity levels appear adequate to detect electromagnetic emissions previously reported and observed at times of seismic activity. Thanks to the efforts made by the DEMETER CNES and industry teams to achieve good EMC performances in particular by ensuring that the external surfaces of the spacecraft and solar panels are conductive and grounded, the interferences are weak and limited to a series of discrete stable frequency lines with a low enough level, even in the HF range, that can be easily eliminated by signal processing on the ground. The instrument has already provided a considerable amount of data of which a few typical examples have been displayed in this paper in order to show its main capabilities.

Acknowledgements

The authors thank the CNES and industry teams who took part in the DEMETER program for their dedication and achievements in designing, building and integrating the satellite. They also want to acknowledge J.P. Lebreton, PI of the ISL experiment, for providing electron density data. This work was supported by funding from CNES under DEMETER/ 736/7621 Grants from 1999 to 2004.

References

Beghin, C., Cerisier, J.C., Rauch, J.L., Berthelier, J.J., Lefeuvre, F., Debrie, R., Molchanov, O.A., Maltseva, O.A., Massevitch, N.I., 1985. Experimental evidence of ELF plasma ducts in the ionospheric trough and in the auroral zone. Adv. Space Res. 5 (4), 229–232.

Berthelier, J.J., Godefroy, M., Leblanc, F., Seran, E., Peschard, D., Gilbert, P., Artru, J., 2005. IAP the thermal plasma analyzer on DEMETER, this issue.

Biagi, P., 1999. Seismic effects on LF radio-waves. In: Hayakawa, A. (Ed.), Atmospheric and Ionospheric Electromagnetic Phenomena Associated with Earthquakes. Terra Scientific Publishing Company, Tokyo, pp. 535–542.

Boccipio, D.J., Williams, E.R., Heckman, S.J., Lyons, W.A., Baker, I.T., Boldi, R., 1995. Sprites, ELF transients and positive ground strokes. Science 269, 1088–1091.

Cerisier, J.C., Berthelier, J.J., Beghin, C., 1985. Unstable density gradients in the high latitude ionosphere. Radio Sci. 20 (4), 755–761.

Dowden, R.L., Brundell, J.B., Lyons, W.A., Nelson, T., 1996. The structure of red sprites and elves determined by VLF scattering, IEEE Antennas Propag. IEEE Antennas Propag. Mag. 38, 7–15.

Engebretson, M.J., Posch, J.L., Halford, A.J., Shelbrune, G.A., Smith, A.J., Spasojevic, A., Inan, U.S., Arnoldy, R.L., 2004. Latitudinal and seasonal variations of quasiperiodic and periodic VLF emissions in the outer magnetosphere. J. Geophys. Res. 109, A05216.

Ergun, R.E., Carlson, C.W., Mozer, F.S., Delory, G.T., Temerin, M., McFadden, J.P., Pankow, D., Abiad, R., Harvey, P., Wilkes, R., Primbsch, H., Elphic, R., Strangeway, R., Pfaff, R., Cattell, C.A., 2001. The FAST Satellite Fields Instrument. Space Sci. Rev. 98, 67–91.

Fraser-Smith, A.C., Bernardi, A., McGill, P.R., Ladd, M.E., Helliwell, R.A., Villard Jr., O.G., 1990. Low-frequency magnetic field measurements near the epicentre of the Ms 7.1 Loma Prieta earthquake. Geophys. Res. Lett. 17, 1465–1468.

Gurnett, D.A., Burns, T.B., 1968. The low frequency cut-off of ELF emissions. J. Geophys. Res. 73, 7437–7445.

Hayakawa, M., 1997. Electromagnetic precursors of earthquakes: review of recent activities. Review Radio Science, 1993–1995. Oxford University Press, Oxford, pp. 807–818.

Hayakawa, M., Molchanov, O.A., Ondoh, T., Kawai, E., 1996. Anomalies in the sub-ionospheric VLF signals for the 1995 Hyogo-ken Nanbu earthquake. J. Phys. Earth, 44, 413–418.

Hayakawa, M., Itoh, T., Hattori, K., Yumoto, K., 2000. ULF electromagnetic precursors for an earthquake at Biak, Indonesia, on February 17, 1996. Geophys. Res. Lett. 27 (10), 1531–1534.

Helliwell, R.A., 1965. Whistlers and related ionospheric phenomena. Stanford University Press, Stanford.

Jacobson, A.R., Knox, S.O., Franz, R.C., Enemark, D.C., 1999. FORTE observations of lightning radio-frequency signatures: capabilities and basic results. Radio Sci. 34, 337.

Jacobson, A.R., Cummins, K.L., Carter, M., Klinger, P., Roussel-Dupre, D., Knox, S.O., 2000. FORTE radio-frequency observations of lightning strokes detected by the National Lightning Detection Network. J. Geophys. Res. 105, 15,653.

Kelley, M.C., Livingstone, R.C., Rino, C.L., Tsunoda, R.T., 1982. The vertical wave number spectrum of topside equatorial spread F: estimates of backscatter levels and implications for a unified theory. J. Geophys. Res. 87, 5217.

Kil, H., Heelis, R.A., 1998. Equatorial density irregularity structures at intermediate scales and their temporal evolution. J. Geophys. Res. 103 (A3), 3969–3981.

LaBelle, J., Kelley, M.C., 1986. The generation of kilometre scale irregularities in equatorial spread F. J. Geophys. Res. 91, 5504.

Labelle, J., Treumann, R.A., 2002. Auroral radio emissions, 1: hisses, roars, and bursts. Space Sci. Rev. 101, 295–440.

Lebreton, J.P., Stverak, S., Travnicek, P., Maksimovic, M., Klinge, D., Merikallio, S., Lagoutte, D., Poirier, B., Kozacek, Z., Salaquarda, M., 2005. The ISL Langmuir Probe experiment and its data processing on board DEMETER: scientific objectives, description and first results.

Lotko, W., Maggs, J.E., 1981. Amplification of electrostatic noise in cyclotron resonance with an adiabatic auroral beam. J. Geophys. Res. 86, 3449–3458.

Molchanov, O.A., Kopytenko, Yu.A., Voronov, P.M., Kopytenko, E.A., Matiashvili, T.G., Fraser-Smith, A.C., Bernardi, A., 1992. Results of ULF magnetic field measurements near the epicentres of the Spitak (Ms = 6.9) and Loma Prieta (Ms = 7.1) earthquakes: comparative analysis. Geophys. Res. Lett. 19, 1495–1498.

Molchanov, O.A., Mazhaeva, O.A., Golyavin, A.N., Hayakawa, M., 1993. Observation by the Intercosmos-24 satellite of ELF-VLF electromagnetic emissions associated with earthquakes. Ann. Geophys. 11, 431–440.

Molchanov, OA., Hayakawa, M., Rafalsky, V.A., 1995. Penetration characteristics of electromagnetic emissions from an underground seismic source into the atmosphere, ionosphere, and magnetosphere. J. Geophys. Res. 100, 1691–1712.

Molchanov, O.A., Hayakawa, M., Ondoh, T., Kawai, E., 1998. Precursory effects in the sub-ionospheric VLF signals for the KOBE earthquake. Phys. Earth Planet. Inter. 105, 239–248.

Mozer, F.S., 1973. Analysis of techniques for measuring DC and AC electric fields in the magnetosphere. Space Sci. Rev. 14, 272.

Nagao, T., Enomoto, Y., Fujinawa, Y., Hata, M., Hayakawa, M., Huang, Q., Izutsu, J., Kushida, Y., Maeda, K., Oike, K., Uyeda, S., Yoshino, T., 2002. Electromagnetic anomalies associated with the 1995 Kobe earthquake. J. Geodyn. 33 (4–5), 349–359.

Ohta, K., Makita, K., Hayakawa, M., 2000. On the association of anomalies in sub-ionospheric VLF propagation at Kasugai with earthquakes in the Tokai area, Japan. J. Atmos. Electr. 20 (2), 85–90.

Parrot, M., Benoist, D., Berthelier, J.J., Blêcki, J., Chapuis, Y., Colin, F., Elie, F., Fergeau, P., Lagoutte, D., Lefeuvre, F., Legendre, C., Lévêque, M., Pinçon, J.L., Poirier, B., Seran, H.-C., Zamora, P., 2005. The magnetic field experiment IMSC and its data processing onboard DEMETER: scientific objectives, description and first results, this issue.

Sakai, K., Takano, T., Shimakura, S., 2001. Observation system for anomalous propagation of FM radio broadcasting wave related to earthquakes and its preliminary results. J. Atmos. Electr. 21 (2), 71–78.

Sato, N., Fukunishi, H., 1981. Interaction between ELF-VLF emissions and magnetic pulsations: classification of quasi-periodic ELF-VLF emissions based on frequency-time spectra. J. Geophys. Res. 86 (A1), 19–29.

Sato, N., Kokobun, S., 1981. Interaction between ELF-VLF emissions and magnetic pulsations: regular period ELF-VLF pulsations and their geomagnetic conjugacy. J. Geophys. Res. 86 (A1), 9–18.

Sazhin, S.S., Hayakawa, M., 1994. Periodic and quasi-periodic VLF emissions. J. Atmos. Terr. Phys. 56 (6), 735–753.

Sentman, D.D., Wescott, E.M., 1993. Observations of upper atmosphere optical flashes recorded from an aircraft. Geophys. Res. Lett. 20, 2857–2860.

Singh, R., Singh, B., Bansal, V., Hayakawa, M., 2000. VLF electromagnetic noise bursts related to major seismic activities observed at Agra. J. Atmos. Electr. 20 (1), 7–20.

Smith, A.J., Engebretson, M.J., Klatt, E.M., Inan, U.S., Arnoldy, R.L., Fukunishi, H., 1998. Periodic and quasi-periodic ELF/VLF emissions observed by an array of Antarctic stations. J. Geophys. Res. 103, 23,611–23,622.

Takano, T., Yamada, A., Sakai, K., Higasa, H., Shimakura, S., 2002. Enhancements of electromagnetic broadband noise in 50 MHz band which possibly associate with earthquakes. J. Atmos. Electr. 22 (1), 23–34.

Tsunoda, R.T., Livingstone, R.C., McClure, J.P., Hanson, W.B., 1982. Equatorial plasma bubbles: vertically elongated wedges from the bottomside F layer. J. Geophys. Res. 87, 9171.

Wu, C.S., Dillenburg, D., Zienbell, L.F., Freund, H.P., 1983. Excitation of whistler waves by reflected auroral electrons. Planet. Space Sci. 31, 499–507.

Yamada, A., Sakai, K., Yaji, Y., Takano, T., Shimakura, S., 2002. Observations of natural noise in VHF band which relates to earthquakes. In: Hayakawa, M., Molchanov, O.A. (Eds.), Seismo Electromagnetics (Lithosphere–Atmosphere–Ionosphere Coupling). Terra Scientific Publishing Company, Tokyo, pp. 255–257.